Atmos. Chem. Phys., 25, 11597–11610, 2025
https://doi.org/10.5194/acp-25-11597-2025

Atmospheric Chemistry and Physics
Open Access
EGU

Molecular insight into aqueous-phase photolysis and photooxidation of water-soluble organic matter emitted from biomass burning and coal combustion

Tao Cao[1,2], Cuncun Xu[1,2,3], Hao Chen[1,2,3], Jianzhong Song[1,2,4], Jun Li[1,2,4], Haiyan Song[5], Bin Jiang[1,2,4], Yin Zhong[1,2,4], and Ping'an Peng[1,2,3,4]

[1]State Key Laboratory of Advanced Environmental Technology, Guangzhou Institute of Geochemistry, Chinese Academy of Sciences, Guangzhou 510640, China
[2]Guangdong Provincial Key Laboratory of Environmental Protection and Resources Utilization, Guangzhou Institute of Geochemistry, Chinese Academy of Sciences, Guangzhou 510640, China
[3]University of Chinese Academy of Sciences, Beijing 100049, China
[4]Guangdong-Hong Kong-Macao Joint Laboratory for Environmental Pollution and Control, Guangzhou 510640, China
[5]School of Chemistry, South China Normal University, Universities Town, Guangzhou 510006, China

Correspondence: Jianzhong Song (songjzh@gig.ac.cn)

Received: 6 February 2025 – Discussion started: 4 March 2025
Revised: 20 June 2025 – Accepted: 11 July 2025 – Published: 30 September 2025

Abstract. Biomass and coal combustion represent substantial contributors to atmospheric water-soluble organic matter (WSOM). This was exposed to intense photochemical oxidation once it entered the atmospheric environment, but the resulting changes in WSOM are largely unclear. This study examines the changes in the optical properties, fluorophores, and molecular composition of WSOM derived from the combustion of biomass, specifically rice straw (RS) and coal from Yulin (YL) during aqueous photolysis and hydroxyl radical (•OH) photooxidation. The results indicate that photochemical aging induces distinct changes in the light-absorbing properties of RS and YL WSOM, characterized by pronounced photobleaching in RS WSOM and photoenhancement in YL WSOM. Additionally, more pronounced alterations were observed during •OH photooxidation than direct photolysis, for both RS and YL WSOM. Furthermore, a greater proportion of molecules in both RS (61.6 %) and YL (65.0 %) WSOM was degraded during •OH photooxidation compared to photolysis (14.9 % and 23.1 %, respectively), resulting in products with a larger molecular weight and higher oxidation levels, including tannin-like substances and newly formed compounds that are similar to black carbon, whereas the products of photolysis were characterized by a relatively minor alteration. These findings provide new insights into the photochemical evolution of combustion-derived WSOM and help to predict its effects in environmental and climatic changes.

1 Introduction

Water-soluble organic matter (WSOM) consists of a diverse array of polar organic species, which is ubiquitous in atmospheric aerosols, cloud, fog, and rainwater (Sun et al., 2023; Wang et al., 2019). WSOM only alters the hygroscopicity and surface tension of aerosol and influence the formation of cloud condensation nuclei but also has significant effects on the radiative forcing of aerosols, thereby playing a crucial role in atmospheric environment and climate change (Sun et al., 2011; Chen et al., 2019; Lee et al., 2022). Due to its high reactivity, WSOM also contributes to atmospheric chemistry and the formation of organic aerosols. Moreover, WSOM has the potential to catalyze a generation of reactive oxygen species, posing adverse impacts to human health (Bhattu et al., 2024; Bates et al., 2019).

Multiple sources of WSOM have been identified, including primary emissions from biomass burning (BB) and coal combustion (CC), vehicular emissions, and secondary formation through the photochemical transformation of volatile organic compounds (Tang et al., 2020; Jiang et al., 2023; Cao et al., 2023). Among these sources, BB has been recognized as a significant contributor to atmospheric WSOM in numerous regions, including East Asia, South East Asia (Liu et al., 2021; Zheng et al., 2017), the Amazon rainforest (Malavelle et al., 2019), and North America (Gallo et al., 2023; Ceamanos et al., 2023). Furthermore, domestic coal combustion also serves as a crucial primary source of atmospheric WSOM in northern China, India (Bikkina et al., 2020; Liu et al., 2022a), and Poland (Casotto et al., 2023). It is important to note that combustion-derived primary WSOM undergoes considerable aging upon entering the atmosphere (Sumlin et al., 2017; Schnitzler et al., 2022). For instance, studies have reported a marked decrease in the light absorption of water-soluble brown carbon (BrC) during transport over distances exceeding 6000 km from the Indo-Gangetic Plain to the Himalayan region (Dasari et al., 2019; Choudhary et al., 2022). Additionally, observations of wildfire plumes in North America have demonstrated a reduction in the mass absorption coefficient as the plume ages (Bali et al., 2024). Nonetheless, the concentrations, light absorption properties, and chemical characteristics of WSOM undergo significant alterations throughout the atmospheric aging process.

Field and laboratory studies have demonstrated that aqueous photochemical processes, including direct photolysis and secondary photochemistry involving oxidants (e.g., hydroxyl radical (•OH), O_3), are ubiquitous and play a significant role in the transformation of atmospheric WSOM (Hems et al., 2021; Manfrin et al., 2019). Research conducted by Cai et al. (2020) revealed that the aqueous photochemistry of BB WSOM can produce highly oxygenated compounds, which subsequently enhance the oxidation state of WSOM in atmospheric samples. Furthermore, the •OH photooxidation of BB-derived organic species (e.g., 4-methylsyringol, eugenol) has been found to form light-absorbing products, indicating a potential pathway for secondary organic aerosol (SOA; Liu et al., 2022a; Li et al., 2023; Arciva et al., 2022). Additionally, the •OH photooxidation of freshly emitted BB WSOM initially results in an increase in its absorption capacity, which is later followed by a photobleaching process during photoaging (Hems et al., 2021; Wong et al., 2017). These findings underscore the dynamic nature of WSOM due to photolytic aging; however, further insights into the molecular transformations leading to these observations remain unclear. Moreover, while the chemical composition of WSOM emitted from BB and CC differs, it remains unclear whether distinct classes of molecules exhibit varying behaviors during photochemical processes.

To address these questions, the photochemical aging of WSOM emitted from both biomass burning and coal combustion was systematically investigated through direct photolysis and OH photooxidation in the aqueous phase. The objectives are (1) to compare the optical evolution of BB and CC WSOM during photolysis and •OH photooxidation and (2) to elucidate the photochemical transformation of BB and CC WSOM at a molecular level using Fourier transform ion cyclotron resonance mass spectrometry (FT-ICR MS). The information obtained will enhance our understanding of the atmospheric oxidation processes of combustion-derived WSOM and their subsequent environmental and climatic effects.

2 Materials and methods

2.1 Preparation of WSOM samples

Rice straw (RS) and Yulin coal (YL) were selected as a representative biomass and coal fuel materials for the preparation of combustion-derived WSOM samples. The detailed information of RS and YL is provided in Sect. S1 and Table S1 in the Supplement. These materials are commonly utilized for heating and cooking in rural households in northern China, particularly during the winter season. Additionally, RS residue is burned in agricultural fields (Zhang et al., 2023; Huang et al., 2022). The smoke samples emitted from the combustion process were collected in a laboratory-controlled combustion system in our laboratory, and more detailed information can be seen in our previous studies (Cao et al., 2021; Li et al., 2018). Immediately after collection, the filters were wrapped with baked aluminum foil and stored in a refrigerator (−20 °C).

Prior to conducting the photolysis and photooxidation experiments, the WSOM fraction was extracted using ultrapure water. Briefly, a filter sample was cut into pieces and placed in a 100 mL glass bottle, to which 60 mL ultrapure water was added. After ultrasonically extracting for 30 min, the extract was filtered through a 0.22 µm polytetrafluoroethylene syringe filter (ANPEL, ANPEL Laboratory Technology (Shanghai) Inc., Shanghai, China). The organic carbon concentration of the WSOM solution was measured by a total organic carbon analyzer (VCPH analyzer, Shimadzu, Kyoto, Japan) following the non-purgeable organic carbon protocol. After the removal of inorganic carbon, the sample was oxidized at a high temperature (680 °C) to generate CO_2 and then determined by a non-dispersive infrared detector. Before the photochemical reaction, the WSOM solution was diluted to 20 mg C L^{-1} by ultrapure water (Gu et al., 2024; Zhang et al., 2022). The detailed information can be found in Sect. S2 in the Supplement.

2.2 Photolysis and •OH photooxidation experiments

The photolysis and •OH photooxidation experiments were conducted in a photoreactor with three replicates, where a quartz cell containing WSOM solution was continuously exposed to radiation. Briefly, 100 mL of 20 mg C L^{-1} WSOM solution was magnetically stirred in a 250 mL cylindrical quartz cell equipped with a water-circulating jacket to maintain a constant temperature of 25 °C. For the photolysis experiment, the WSOM solution was irradiated from the top by a Xenon lamp (PL-XQ500W, Beijing Princess Technology Co. Ltd, Beijing, China), with an output energy of 500 W at 0.2 m. The irradiation energy at the water surface is 12.5 mW cm^{-2} (290–400 nm), which is about 5.2 times higher than the light intensity of actual solar exposure (Fig. S1 in the Supplement, obtained at noon on 20 May 2023, Guangzhou). The actinic flux of the Xenon lamp is 5.4×10^{-5} Einstein cm^{-2} s^{-1}, as determined by the p-nitroanisole/pyridine actinometer method (Laszakovits et al., 2016). For the •OH photooxidation experiments, 3 mM H_2O_2 was added to the WSOM solution as a photolytic source of •OH radicals upon irradiation (Zhao et al., 2015; Fan et al., 2023; Arciva et al., 2024). Based on the conditional experiment, it was found that approximately 35.6 % ± 4.6 % of H_2O_2 was consumed after a 24 h reaction period. This indicates that there was a sufficient amount of •OH present to react with WSOM during the •OH photooxidation experiment. For each experiment, 4 mL samples were withdrawn periodically (0, 1, 2, 4, 8, 12, and 24 h) from the reactor and then diluted to 20 mL for further analysis. The photolysis and •OH photooxidation experiment were both carried out synchronously during the dark control, following the conditions as introduced above. The results showed that no significant changes were observed for the organic carbon content and the ultraviolet–visible (UV–vis) absorption of WSOM within the reaction time.

2.3 Spectroscopy measurement

The UV–vis absorption of WSOM was measured using a UV–vis spectrophotometer (UV-2600i, Shimadzu, Japan) within the wavelength range of 200–700 nm. Excitation-emission matrix (EEM) spectra were recorded by a 3D fluorescence spectrophotometer (Aqualog, HORIBA Scientific, Irvine, CA, US). The scanning ranges for excitation (Ex) and emission (Em) were 240–800 nm and 250–800 nm, respectively. Ultrapure water (18.2 MΩ cm^{-1}) was used as a blank reference, and the fluorescence intensity unit was normalized by the Raman peak area of water (R.U.). In addition, the corresponding absorption spectra were used to correct the EEM for inner-filter effects (IFEs), according to previous studies if the absorbance is higher than 0.05 at 250 nm (Tang et al., 2020; He and Hur, 2015; Murphy et al., 2013). The PARAFAC modeling procedure was conducted in MATLAB 2021b (MathWorks, Inc., Natick, MA, US) using the drEEM toolkit (Murphy et al., 2018; Pucher et al., 2019). More information and data processing details are provided in Sect. S3 in the Supplement.

2.4 High-resolution mass spectrometry analysis

The molecular characteristics of WSOM before and after photolysis and •OH photooxidation were measured with a solariX XR FT-ICR MS (Bruker Daltonik GmbH, Bremen, Germany) equipped with a 9.4 T refrigerated actively shielded superconducting magnet and a ParaCell analyzer cell. The WSOM samples used for the FT-ICR MS analysis were desalted by a solid-phase extraction cartridge (Oasis HLB, 200 mg, Waters, Milford, MA, US) as introduced in our previous studies (Song et al., 2019, 2018, 2022). The detailed measurement condition and the calculation of corresponding indexes (e.g., double bond equivalent (DBE) and a modified aromaticity index (AI_{mod})) are described in Sect. S4 in the Supplement. To better elucidate the transformation of RS and YL WSOM, the photochemically resistant, degraded, and produced molecules were investigated (Fan et al., 2024; Gu et al., 2024).

3 Results and discussion

3.1 Effect of photolysis and •OH photooxidation on the light absorption of WSOM

The absorption spectra of RS and YL WSOM during photolysis and •OH photooxidation are illustrated in Fig. 1a–d. It can be observed that the absorbance of RS WSOM gradually decreases as aging time increases during both photolysis and •OH photooxidation, indicating substantial photobleaching (Fan et al., 2024; Zhao et al., 2022). Moreover, the reduction in absorbance during •OH photooxidation is more obvious than in photolysis, indicating that RS WSOM undergoes greater degradation during •OH photooxidation. In contrast, the absorbance of YL WSOM presents a differing variation during photolysis and •OH photooxidation. Specifically, the absorbance in the short wavelength range of 210–240 nm decreases gradually with aging time, while the absorbances at wavelengths exceeding 360 nm increase. This phenomenon is characteristic of photoenhancement, which aligns with the findings reported in previous studies concerning the nitrate-mediated photooxidation of guaiacol and 5-nitroguaiacol and the photooxidation of mixed aromatic carbonyls (Go et al., 2024; Yang et al., 2021).

To quantitatively assess the changes in light-absorbing substances during photolysis and •OH photooxidation, the absorption coefficients at 254 nm (α_{254}) and 365 nm (α_{365}) were calculated (Fan et al., 2024; Zou et al., 2023). As shown in Fig. 1e, the α_{254} values for both RS and YL WSOM consistently decline during photolysis and •OH photooxidation, with a more significant reduction observed during •OH photooxidation. These results are consistent with earlier studies

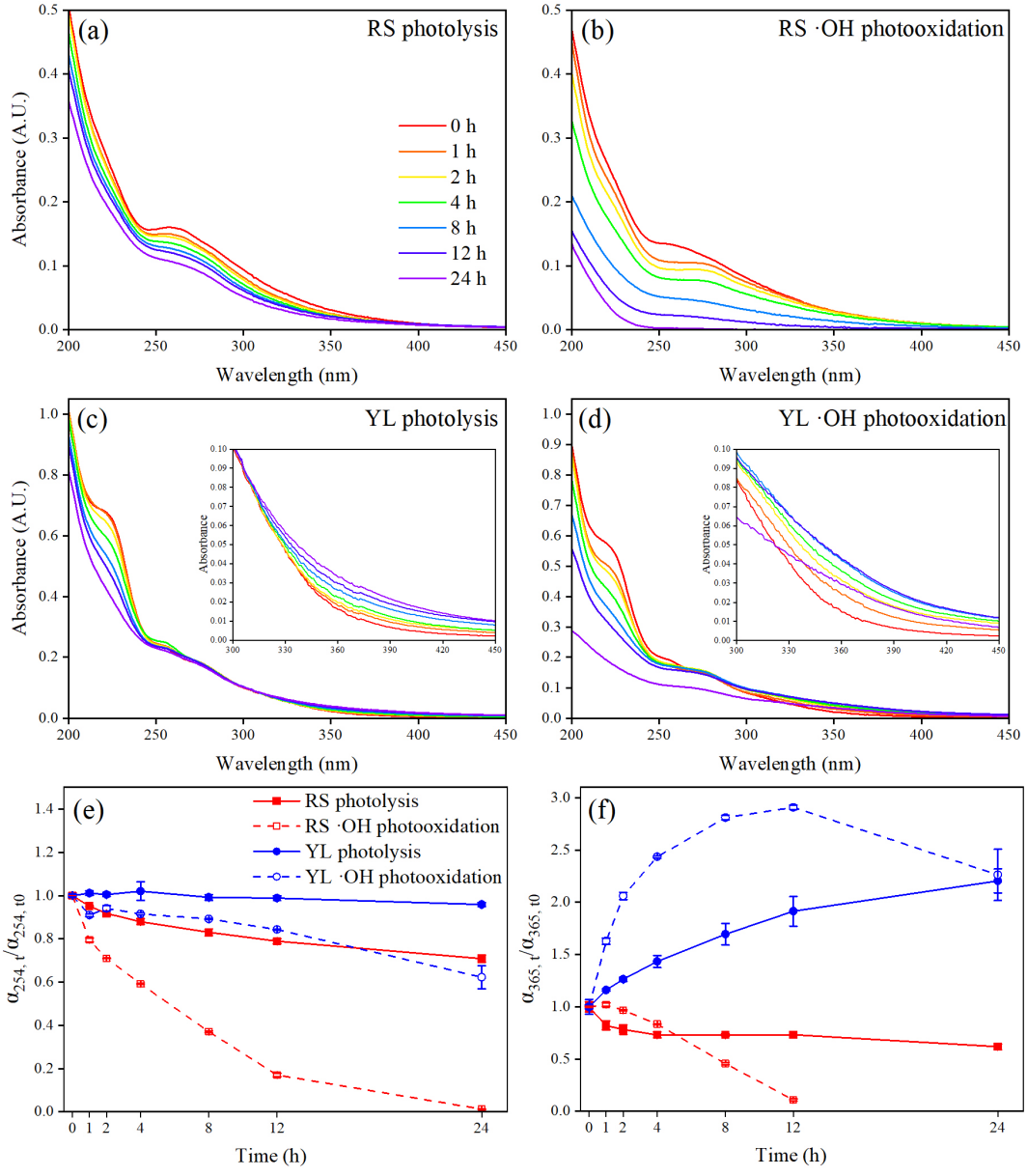

Figure 1. UV–vis spectra of RS and YL WSOM during photolysis **(a, c)** and •OH photooxidation **(b, d)**. The inserted figures in **c** and **d** represent UV–vis spectra in the wavelength range 300–450 nm of YL WSOM during photolysis and •OH photooxidation. Changes in α_{254} **(e)** and α_{365} **(f)** of RS and YL WSOM during photolysis and •OH photooxidation. The error bars represent 1 standard deviation ($\pm 1\sigma$) of the triplicate samples.

on the dark •OH oxidation of BB WSOM, indicating that the presence of •OH radicals accelerates the degradation of aromatic structures in WSOM (Fan et al., 2024; Ye et al., 2020). Additionally, the reduction of α_{254} values was always greater for RS WSOM than for YL WSOM, suggesting that RS WSOM is more susceptible to photochemical degradation.

The α_{365} values for RS and YL WSOM exhibit different variations during photolysis and •OH photooxidation. As illustrated in Fig. 1f, the α_{365} value for RS WSOM gradually decreases with prolonged photolysis, while it initially increased slightly before decreasing during •OH photooxidation. A similar observation has been made in the photochemical aging of wood smoke BrC and monomeric phenolic compounds, suggesting the formation of new compounds with significant light-absorbing capacity during the initial stage of the •OH photochemical reaction (Hems et al., 2021; Wong et

al., 2017; Lee et al., 2014). In contrast, the α_{365} values of YL WSOM presented markedly different trends, increasing during 24 h photolysis and initially rising for 12 h before decreasing from 12 to 24 h during •OH photooxidation. These results indicate that the products generated from the photochemical reaction of YL WSOM possess enhanced light absorbance in the near-UV and visible regions, which are also observed in the aqueous-phase oxidation of aromatic compounds such as phenols (Arciva et al., 2024; Smith et al., 2016). The proposed mechanism may involve the aromatization of phenolic compounds and the •OH functionalization of aromatic compounds, leading to the formation of strong light-absorbing substances at a longer wavelength (Li et al., 2023).

3.2 EEM-PARAFAC of WSOM during the photolysis and •OH photooxidation

The EEM-PARAFAC model has successfully identified three distinct fluorescent components (C1–C3) in RS and YL WSOM. As shown in Fig. 2a, C1 displays excitation/emission peaks at Ex/Em = 270/325 nm, which are attributed to protein-like substances, including tyrosine-like substances (Podgorski et al., 2018; Hu et al., 2023), as well as non-nitrogenous-containing species such as phenol-like compounds (Cao et al., 2023). C2 (240, 320/420 nm) and C3 (240/350 nm) are both assigned to humic-like substances (Hu et al., 2023; He et al., 2023; Fan et al., 2021). Fluorophores observed at longer wavelengths are primarily attributed to organic substances with high molecular weight and a great degree of oxygenation (Cao et al., 2023). This suggests that the longer emission wavelengths of C2 might be associated with highly oxygenated humic-like fluorophores with a higher molecular weight and aromaticity, while C3 could be more relevant to less oxygenated structures and conjugated systems. Furthermore, fluorophores contain the same position as C2 and have been observed during the photooxidation of vanillic acid and the ozone oxidation of BB BrC (Fan et al., 2021; Tang et al., 2020), indicating that C2 may be closely related to the products formed through atmospheric oxidation processes.

To quantitatively access the changes in the distribution of fluorophores during the photochemical process, total fluorescence intensity (TFI) was calculated. As depicted in Fig. 2d, the TFI values for RS and YL WSOM showed a comparable decline during both photolysis and •OH photooxidation, with a pronounced reduction during •OH photooxidation. These results indicate that fluorophores are more susceptible to degradation or quenching by •OH attacks than by direct photolysis in both BB and CC WSOM. On the one hand, more aromatic structures in WSOM may be disrupted by the •OH radical, resulting a more significant reduction in fluorophores. On the other hand, the •OH photooxidation also leads to an increase in carboxyl groups, which are the typical electron-withdrawing groups, thereby contributing to a reduction or quenching of fluorescence in WSOM.

Moreover, the relative contribution of the three fluorophores in RS and YL WSOM varied throughout the photochemical processes, with more significant changes noted during •OH photooxidation (Fig. 2e–h). It is clear that the increases in C2 are 49 % and 56 % for RS and YL WSOM, respectively, during •OH photooxidation, which is significantly higher than that 5 % and 14 % during photolysis. This can be explained by the formation of more highly oxygenated humic-like fluorophores due to •OH photooxidation (Zhang et al., 2022; Fan et al., 2024). In contrast, fluorophore C3 greatly declined by 35 % and 56 % for RS and YL WSOM, respectively, during •OH photooxidation. Previous studies have linked fluorophore C3 to less-oxygenated fluorescent substances resulting from primary combustion (Cao et al., 2023; Chen et al., 2016), which can be oxidized and gradually removed during the •OH photooxidation process. Comparatively, the contributions of three fluorescent components in RS and YL WSOM both display relatively minor variations during photolysis, suggesting a lower selectivity of photolysis. These notable variations in both the subgroup and intensity of fluorophores suggest their potential utility as an indicator of the atmospheric oxidation processes experienced by fresh emissions (Fan et al., 2024; Ye et al., 2025).

3.3 Changes in molecular characteristics of RS and YL WSOM

Figure 3 shows the FT-ICR MS spectra of RS and YL WSOM before and after undergoing photochemical oxidation. A total of 5114 to 6383 molecules were identified within the m/z range of 100–600, with a predominant concentration of peaks observed between 150 and 400. These findings are indicative of the molecular characteristics typical of organic compounds resulting from BB and coal combustion emissions (Tang et al., 2020; Song et al., 2018, 2022). The identified formulae were categorized into four groups based on their elemental composition: CHO, CHON, CHOS, and CHONS (Tang et al., 2020; Song et al., 2018). As shown in Fig. 3, CHO and CHON compounds are the dominant compounds (95.8 %–98.4 %) in RS WSOM, with minor fluctuations following photolysis and •OH photooxidation. Similar changes were also observed for BB WSOM during dark •OH oxidation (Fan et al., 2024). In contrast to RS WSOM, YL WSOM contains not only a high content of CHO (47.6 %) and CHON (33.1 %) but also significant S-containing substances (CHOS and CHONS, 19.2 %). Figure 3 reveals notable differences in the composition of compound groups within YL WSOM. The CHO compounds in fresh YL WSOM are 47.6 %, which increased to 76.1 % and 84.2 % after photolysis and •OH photooxidation, respectively. Meanwhile, the CHON compounds decreased from 33.1 % to 13.4 % and 13.6 %, respectively. Additionally, S-containing compounds demonstrated a marked decrease fol-

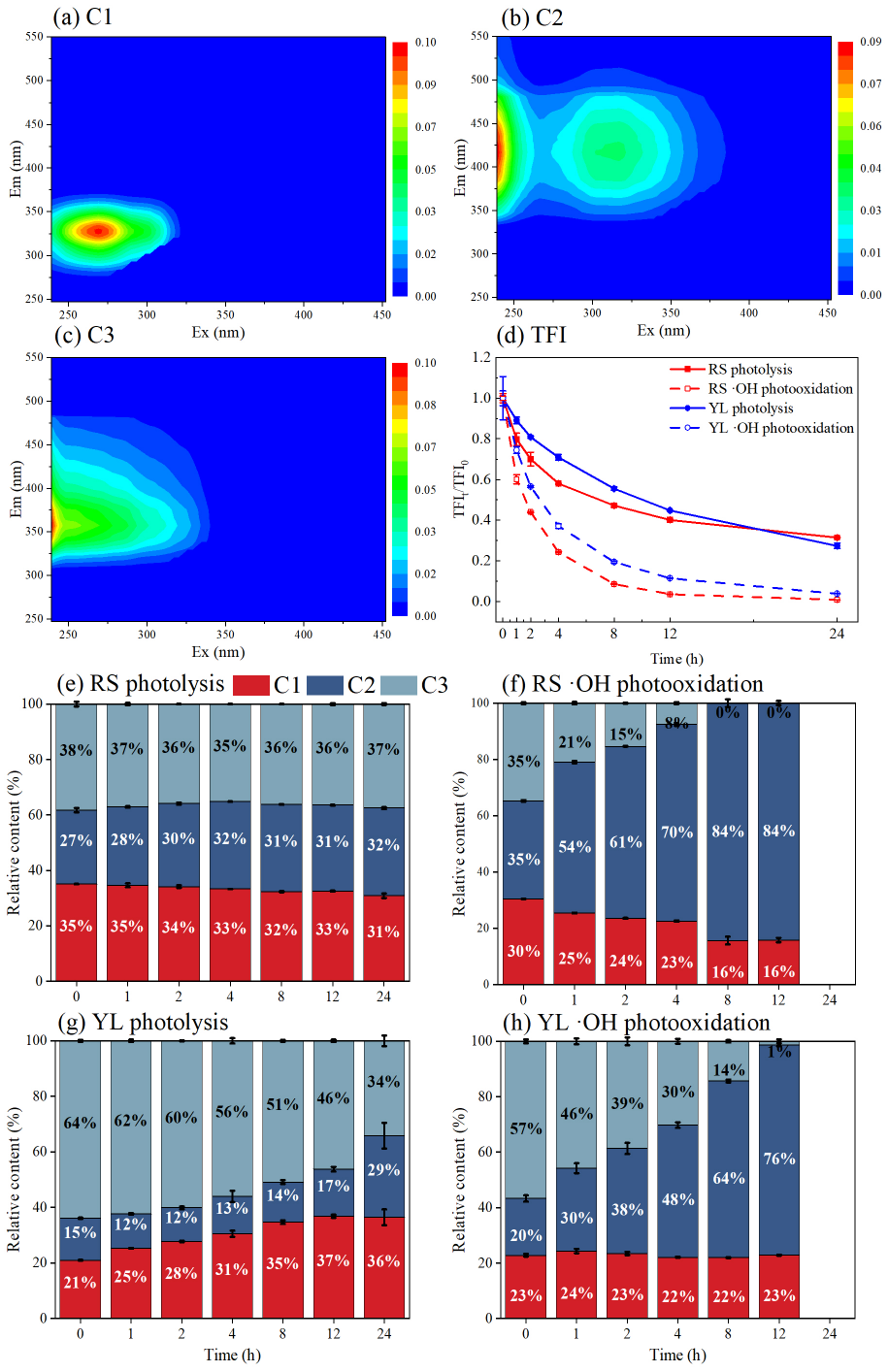

Figure 2. **(a–c)** Excitation–emission matrix (EEM) spectra of PARAFAC-derived fluorescence components (C1–C3) in RS and YL WSOM. Changes in total fluorescence intensity (TFI) **(d)** and the relative content of three individual fluorescence component in RS and YL WSOM during photolysis and •OH photooxidation **(e–h)**. The error bars represent 1 standard deviation ($\pm 1\sigma$) of the triplicate samples.

lowing photolysis and •OH photooxidation for YL WSOM. These discrepancies may be attributed to the inherent differences in molecular composition between RS WSOM and YL WSOM, which exhibit varying sensitivities to photolysis and •OH photooxidation.

3.3.1 Molecular properties

The intensity-weighted average values of various molecular parameters, including molecular weight (MW_w), elemental ratios, double bond equivalents (DBE_w), modified aro-

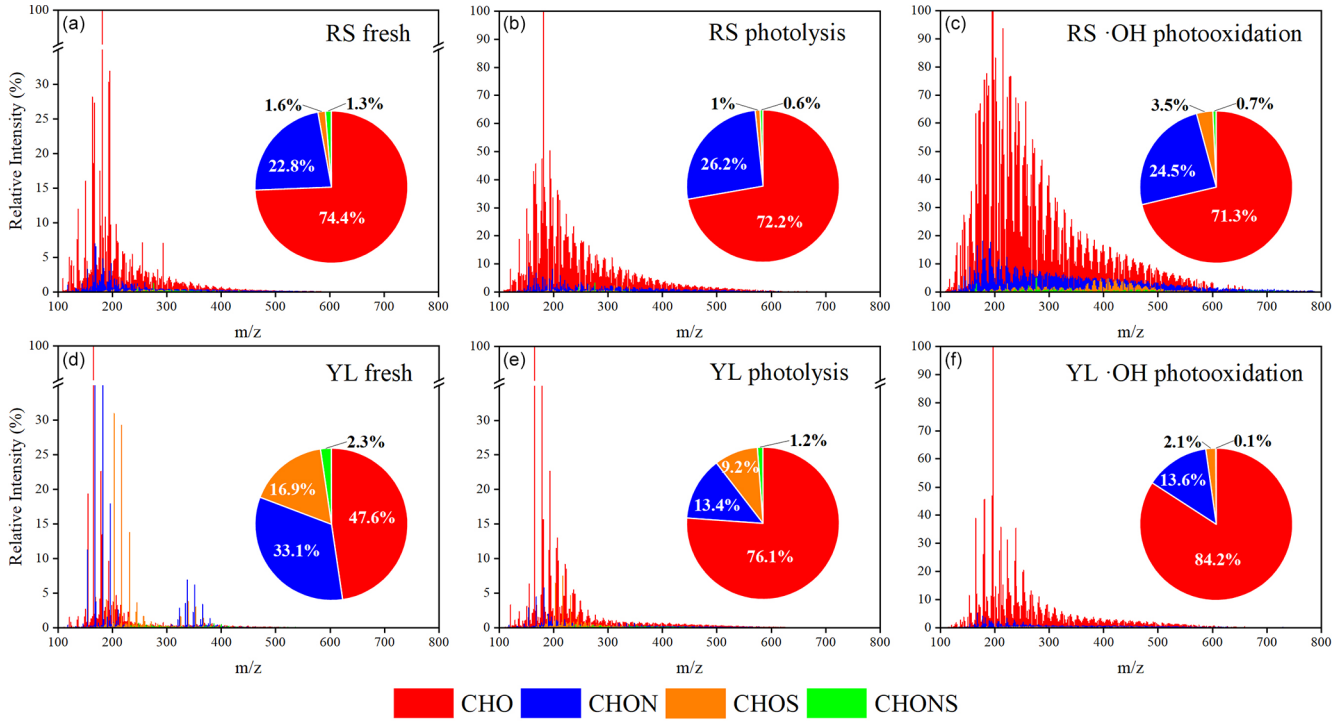

Figure 3. Reconstructed mass spectra of RS and YL WSOM for fresh **(a, d)**, photolysis **(b, e)**, and •OH photooxidation **(c, f)**. Pie charts inserted represent the relative content of different formula groups in each sample by the sum of intensities of all identified peaks.

maticity index ($AI_{mod,w}$), and nominal oxidation state of carbon ($NOSC_w$), of RS and YL WSOM before and after photochemical aging are summarized in Table S2 in the Supplement. It is evident that the molecular characteristics of WSOM underwent significant alterations following photolysis and •OH photooxidation. Specifically, the MW_w value of fresh RS WSOM is 252, which increased to 288 and 319 after photolysis and •OH photooxidation, respectively. A similar trend was observed for YL WSOM, where the MW_w values increased from 231 to 268 and 303 after photolysis and •OH photooxidation, respectively. These observations in molecular weight aligned with findings related to the aqueous-phase photochemical oxidation of wood smoke WSOM, but no significant change in molecular weight was observed in the aqueous-phase dark •OH oxidation of BB WSOM (Fan et al., 2024; Wong et al., 2019). Such changes may be attributed to the new formation of higher MW molecules through the oligomerization reactions and the resistance of high-MW molecules during photochemical aging (Gu et al., 2024; Fan et al., 2024; Go et al., 2024; Waggoner et al., 2015; Carena et al., 2023). Furthermore, it is noteworthy that the MW_w values for both RS and YL WSOM following •OH photooxidation were greater than that after photolysis, suggesting that •OH photooxidation exerts a more pronounced aging effect.

As detailed in Table S2, the $AI_{mod,w}$ value of fresh RS WSOM is 0.44, which subsequently decreased to 0.42 and 0.36 after photolysis and •OH photooxidation, respectively. A similar variation was noted for YL WSOM, where the $AI_{mod,w}$ value decreased from 0.56 to 0.52 and 0.47 after photolysis and •OH photooxidation, respectively. Moreover, the reduction in $AI_{mod,w}$ values was more pronounced for both RS and YL WSOM after being subjected to •OH photooxidation. This significant decrease in the $AI_{mod,w}$ values of BB WSOM was also observed during dark •OH oxidation (Fan et al., 2024). These results indicate that the aromatic structures within WSOM are disrupted during photochemical processes, while •OH photooxidation results in a more significant breakdown (Zhao et al., 2022).

The O/C_w and $NOSC_w$ values were used to estimate the oxidation degree of the formulae in WSOM. As shown in Table S2, the O/C_w of RS WSOM increased from 0.38 to 0.43 and 0.59 after photolysis and •OH photooxidation, respectively, indicating an increase in the number of oxygen atoms within the molecules post-oxidation. Notably, the $NOSC_w$ values exhibited a similar trend to that of O/C_w. These observations are consistent with the findings related to BB WSOM during dark •OH oxidation and the photochemical transformation of DOM (Gu et al., 2024; Zhang et al., 2022; Fan et al., 2024). This suggests a substantial incorporation of O-containing functional groups into carbon structures during photolysis and •OH oxidation. The O/C_w and $NOSC_w$ values for YL WSOM demonstrated analogous changes following •OH photooxidation, increasing from 0.46 to 0.57 and from 0.06 to 0.14, respectively. However, the O/C_w and $NOSC_w$

values for YL WSOM exhibit a slight decrease after photolysis, declining from 0.46 to 0.43 and from 0.06 to −0.09, respectively. These findings indicate that the photochemical evolution of WSOM is significantly influenced by its molecular composition. Nonetheless, it is undoubtedly clear that the O/C_w and $NOSC_w$ values of aged WSOM resulting from •OH photooxidation are significantly higher than those resulting from photolysis, indicating a more robust oxidation process.

To further elucidate the molecular distribution of WSOM, Van Krevelen (VK) diagrams were constructed by plotting the H/C ratio versus the O/C ratio. As indicated in Fig. S2 in the Supplement, the identified compounds are classified into seven distinct regions (Sun et al., 2023; Song et al., 2018): (I) lipid-like, (II) protein/amino sugars, (III) carbohydrate-like, (IV) unsaturated hydrocarbons, (V) lignin/CRAM-like, (VI) condensed aromatic, and (VII) tannins. It is obvious that lignin/CRAM-like compounds emerged as the predominant constituents, comprising 83.1 % and 88.4 % of the fresh RS and YL WSOM, respectively (Table S3 in the Supplement). The proportion of these compounds remained stable following photolysis; however, a decline was observed following •OH photooxidation, with the contents decreasing from 83.1 % to 63.3 % for RS WSOM and from 88.4 % to 73.9 % for YL WSOM. Lipid compounds were also identified in both fresh RS and YL WSOM, with relative higher contents in RS WSOM; however, a significant reduction in lipid content was noted after •OH photooxidation for both RS WSOM and YL WSOM. This trend aligns with observations of DOM under UV irradiation, where lignin and lipids were identified as the most active component involved in molecular conversion (Gu et al., 2024). Conversely, the content of tannin-like substances in both RS and YL WSOM greatly increased due to •OH photooxidation. This suggests that the attack by the •OH radical leads to the formation of more polar tannin compounds, indicating the potential contribution of multiple oxygen-enriched groups (i.e., carboxyl) to the aged WSOM. Such additional functional groups may enhance the polarity and reactivity of WSOM, thereby influencing their optical properties, chemical reactivity, and interactions with other atmospheric components. It is noteworthy that more condensed aromatic compounds were observed in aged WSOM subjected to photochemical process, especially •OH photooxidation (e.g., the left and bottom of the VK diagrams, Fig. S2). Furthermore, as shown in Table S3, the content of condensed aromatic compounds increased from 1.08 % to 1.55 % and 4.86 % (RS WSOM) and from 2.86 % to 4.08 % and 5.38 % (YL WSOM) after photolysis and •OH photooxidation, respectively. These findings strongly support the notion that condensed aromatic molecules are formed through photochemical reactions, particularly the •OH photooxidation reaction.

3.3.2 Comparison of the transformation of WSOM, induced by photolysis and •OH photooxidation

To enhance the understanding of molecular transformations occurring in RS and YL WSOM, the photochemically resistant, degraded, and produced molecules were investigated. The formulae identified both before and after photochemical aging were assigned to resistant, unique formulae before a reaction represented the degraded molecules, and unique formulae after the reaction were considered for newly produced molecules (Fig. 4) (Gu et al., 2024; Fan et al., 2024; Zhao et al., 2022). It is important to acknowledge that the molecules categorized as resistant may also include those generated from the photochemical reaction but with the formulae of those in fresh molecules. As presented in Table S4 in the Supplement, approximately 14.9 % of the total number of formulae in fresh RS WSOM and 23.1 % in YL WSOM were degraded through photolysis, resulting in the formation of 26.0 % (RS WSOM) and 31.7 % (YL WSOM) of newly produced formulae in the aged WSOM, respectively. In contrast, a much higher content of formulae (61.6 % of RS WSOM and 65.0 % of YL WSOM) were degraded by •OH photooxidation and led to a higher content (57.0 %–61.0 %) of new formulae. These findings suggest that •OH photooxidation possesses greater oxidative potential, resulting in a more substantial degradation and transformation of molecules.

As shown in Fig. 4b, e, h, and k, the majority of the degraded molecules were found in regions characterized by O/C (< 0.6) in the VK diagram. In contrast, the newly produced molecules were concentrated in the regions of $0.3 < O/C < 0.9$. This finding implies that molecules with low O/C underwent oxidation during the photolysis and •OH photooxidation processes, resulting in their transformation into oxygen-enriched structures, especially through •OH photooxidation. Furthermore, notable differences were observed in the VK diagrams corresponding to photolysis and •OH photooxidation. It is clear that the degraded molecules from RS and YL WSOM were distributed in the same region of the VK diagrams; however, the newly formed molecules resulting from distinct photochemical reactions were distributed across different regions (Fig. S3 in the Supplement). For example, the molecules produced from the photolysis of RS WSOM are located primarily in the range of $0.3 < O/C < 0.7$ and $0.5 < H/C < 1.7$, whereas those generated through •OH photooxidation were found in two separate regions. The majority of these molecules were concentrated in the range $0.4 < O/C < 0.9$ and $0.4 < H/C < 2.0$, indicating a higher formation of oxygenated compounds through •OH photooxidation. As illustrated in Fig. 4f and l, the presence of tannin-like compounds in the molecules produced after •OH photooxidation was much higher than that formed after photolysis for both RS and YL WSOM. These results indicate that the •OH photooxidation process substantially enhanced the abundance of O-containing functional

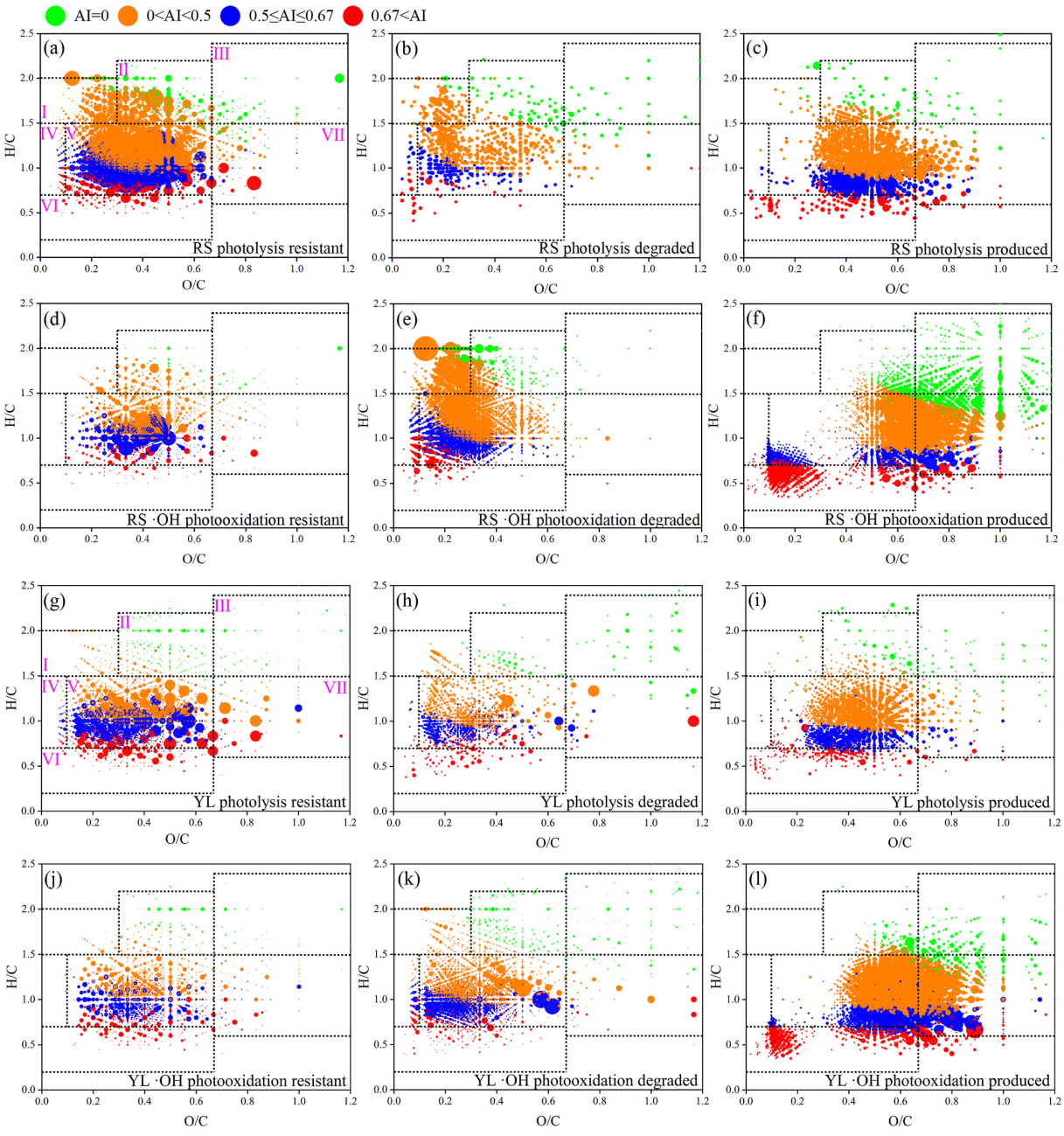

Figure 4. Van Krevelen diagrams for molecules that are resistant, degraded, and produced after photolysis and •OH photooxidation for RS WSOM (upper) and YL WSOM (bottom).

groups within the molecules, as well as the overall oxidation state of WSOM. Additionally, certain condensed aromatic molecules were identified in the region VI in Figs. 4f and l and S2, showing the new production of condensed aromatics during •OH photooxidation. According to Table S5 in the Supplement, these newly formed condensed molecules were identified in both RS and YL WSOM, accounting for 11.6 % and 4.7 % of the total produced molecules (intensity weighted). These compounds exhibited lower H/C_w (0.55 and 0.60) and O/C_w (0.14 and 0.17) ratios alongside higher $AI_{mod,w}$ (0.76 and 0.77) values, indicating a predominance of highly aromatic structures. Moreover, they consisted of CHO, CHON, CHOS, and CHONS, among which CHON is the highest component (57.7 % and 58.0 %) for both RS and YL WSOM. It is noteworthy that the O/N_w ratios for CHON and the O/S_w ratios for CHOS were relatively low, suggesting that the N-containing and S-containing functional group here mainly comprise reduced groups. According to previous

studies, condensed aromatic compounds are usually assigned to traditional dissolved black carbon (BC) molecules derived from combustion (Fan et al., 2023; Liu et al., 2022b; Yan et al., 2022). These compounds share similar molecular characteristics, such as lower H/C_w ratios and higher $AI_{mod,w}$ values. However, our study suggests that •OH photochemical oxidation may also contribute to the formation of BC-like molecules. In contrast, without the presence of light (initiated by Fenton chemistry), the •OH oxidation does not produce these BC-like substances (Fan et al., 2024). This possibly indicates that the formation of highly aromatic BC-like molecules requires both •OH oxidation and photoreactions to occur.

As shown in Table S6 in the Supplement, the degraded molecules exhibited lower $AI_{mod,w}$ values and O/C_w ratio and higher MW_w, DBE_w, and H/C_w values compared to the resistant molecules. For example, the $AI_{mod,w}$ value and O/C_w ratio of the degraded molecules of RS WSOM are 0.33 and 0.33, respectively, which are lower than the corresponding values of 0.38 and 0.45 for the resistant molecules during photolysis. Conversely, the MW_w, DBE_w, and H/C_w ratios for the degraded molecules are 392, 8.3, and 1.29, respectively, significantly higher than that of the resistant molecules. Similar differences were noted between the resistant and degraded molecules in RS WSOM subjected to •OH photooxidation, as well as in YL WSOM that underwent both photolysis and •OH photooxidation. These differences indicate that the WSOM that is susceptible to photochemical aging is those molecules with a higher molecular weight, double bond intensity, and aliphatic structures but with a lower aromaticity and O-containing groups.

In comparison, the newly formed molecules within RS and YL WSOM demonstrate elevated O/C_w, DBE_w, and MW_w values. For example, the newly formed molecules for RS WSOM resulting from photolysis possess higher O/C_w (0.48), DBE_w (12.0), and MW_w (473) than the degraded molecules. These results indicate that photolysis generates a greater quantity of high-molecular-weight compounds, which also contain more oxygenated functional groups, such as carbonyl. Furthermore, the differences between the degraded and resistant molecules during •OH photooxidation are more pronounced than that during the photolysis process, suggesting that a more extensive aging reaction occurs during •OH photooxidation. However, the variation in $AI_{mod,w}$ value between the degraded and produced molecules differs across samples. In the case of RS WSOM, the produced molecules exhibit higher $AI_{mod,w}$ values than the degraded molecules during the photolysis process, yet they are very similar during •OH photooxidation. Additionally, distinct changes in $AI_{mod,w}$ values were observed for YL WSOM during photolysis, where the $AI_{mod,w}$ value of newly produced molecules is lower than that of degraded molecules, and the proportion of aromatic and condensed aromatic compounds decreased for YL WSOM after photolysis. These discrepancies may be due to the produced molecules defined representing only a subset of those generated during the aging process.

3.4 Comparison of the photochemical evolution of WSOM from biomass burning and coal combustion

The photochemical evolution of WSOM originating from BB and CC was comparably investigated in our study. Our results indicate that the absorption spectra of RS and YL WSOM exhibit a decreasing trend at ranges below 240 nm during photolysis and •OH photooxidation. However, notable differences were observed between the two types of WSOM. For example, the α_{365} value for RS WSOM consistently decreased throughout the photolysis and •OH photooxidation, whereas YL WSOM displayed a progressive increase in this value. These differences may be attributed to the inherent differences in WSOM derived from biomass burning compared to that from coal combustion (Cao et al., 2021; Song et al., 2018). The results indicate that WSOM derived from various sources may undergo distinct changes in absorbance during photochemical aging, potentially leading to varying impacts on climate change and radiation balance.

Furthermore, the TFI values for both RS and YL WSOM exhibit a gradual decline during photolysis and •OH photooxidation, with no significant differences between the two. However, the variations in fluorophore composition in RS and YL WSOM were markedly different. For example, three fluorophores in RS WSOM remained relative stable during photolysis, while the less-oxygenated fluorophores C3 in YL WSOM gradually decreased. This may indicate that the fluorophores C3 in YL WSOM are more susceptible to photolytic degradation. These results suggest that the molecular composition of identical fluorescent components in WSOM derived from different sources may exhibit notable differences.

As previously discussed, there are notable similarities in the molecular alterations observed in RS and YL WSOM after photolysis aging. Specifically, the MW_w values for both RS and YL WSOM exhibited an increase after photochemical processes, suggesting the formation of high-MW molecules through the oligomerization reaction and the resistance of high-MW molecules during photochemical aging. Furthermore, the $AI_{mod,w}$ values always decreased, while the O/C ratios consistently increased for both aged RS and YL WSOM. These results indicate the breakdown of aromatic structures and the formation of O-containing groups in WSOM as a result of photochemical processes. However, distinct differences in molecular characteristics between RS and YL WSOM were observed, which may influence their respective changes due to photochemical reactions. For example, CHON compounds in RS WSOM exhibit a minor variation after photochemical reactions, whereas this greatly decreased in YL WSOM. Notably, RS WSOM experienced a greater degradation of lipids during photolysis and •OH photooxidation, leading to the production of carbohydrates or tannin-like substances (Table S3).

4 Environmental significance

Biomass and coal combustion releases considerable quantities of WSOM into the atmosphere, which undergoes significant photochemical transformations under light irradiation, resulting in considerable uncertainty regarding its physical and chemical characteristics, as well as reactivity in the atmospheric environment. The present study investigated the optical and molecular evolution in WSOM derived from BB and CC (i.e., RS and YL WSOM) during aqueous-phase photolysis and •OH photooxidation. The findings indicate a marked reduction in light absorption of RS WSOM at 365 nm during photochemical processes, which is more pronounced for •OH photooxidation, indicating a stronger photobleaching. In contrast, a notable photoenhancement was observed for YL WSOM during the photochemical processes. These results suggest that the alteration in the light absorption of WSOM is closely linked to the chemical composition of fresh WSOM.

At the molecular level, the degradation of aromatic structures in WSOM was evident, accompanied by the formation of O-containing polar groups (e.g., carbonyl, carboxyl groups), as a result of the photochemical reactions, particularly during •OH photooxidation. These results indicate that the oxidation degree and severity of •OH photooxidation is much higher than that of photolysis, leading to the variations in the optical properties of WSOM. It is worth noting that the polymerization occurs in both photolysis and •OH photooxidation, especially in •OH photooxidation, as evidenced by an increase in MW_w and the formation of condensed aromatic compounds. These condensed aromatic compounds exhibit similarities to the chemical and molecular structures of combustion-derived BC molecules. Therefore, •OH photochemical oxidation may be a potential formation mechanism of BC-like materials.

It is important to note that this study focused solely on WSOM produced from a specific type of biomass and coal samples in a laboratory-type simulated system, which may not accurately reflect the complexities of combustion processes in real-world scenarios. Therefore, a more comprehensive investigation into the photochemical aging of WSOM from diverse biomass and coal sources, as well as under various conditions in natural environments, is warranted. Furthermore, it is clear that the photochemical aging processes significantly influence the environmental, climate, and health effects, necessitating further exploration in future research endeavors.

Data availability. The research data used in this study are available from Jianzhong Song (songjzh@gig.ac.cn).

Supplement. The supplement related to this article is available online at https://doi.org/10.5194/acp-25-11597-2025-supplement.

Author contributions. TC and JS designed the research and wrote the paper. TC, CX, HC, and HS analyzed the combustion-derived WSOM samples during photochemical process. BJ analyzed the WSOM samples by FT-ICR MS. JL, YZ, and PP commented on and revised the paper.

Competing interests. The contact author has declared that none of the authors has any competing interests.

Disclaimer. Publisher's note: Copernicus Publications remains neutral with regard to jurisdictional claims made in the text, published maps, institutional affiliations, or any other geographical representation in this paper. While Copernicus Publications makes every effort to include appropriate place names, the final responsibility lies with the authors.

Acknowledgements. This is contribution no. IS-3704 from GIGCAS.

Financial support. This study was supported by the National Natural Science Foundation of China (42192514), the Guangdong Major Project of Basic and Applied Basic Research (2023B0303000007), and the Guangdong Foundation for the Program of Science and Technology Research (2023B1212060049).

Review statement. This paper was edited by Joachim Curtius and reviewed by two anonymous referees.

References

Arciva, S., Niedek, C., Mavis, C., Yoon, M., Sanchez, M. E., Zhang, Q., and Anastasio, C.: Aqueous •OH Oxidation of Highly Substituted Phenols as a Source of Secondary Organic Aerosol, Environ. Sci. Technol., 56, 9959–9967, https://doi.org/10.1021/acs.est.2c02225, 2022.

Arciva, S., Ma, L., Mavis, C., Guzman, C., and Anastasio, C.: Formation and loss of light absorbance by phenolic aqueous SOA by •OH and an organic triplet excited state, Atmos. Chem. Phys., 24, 4473–4485, https://doi.org/10.5194/acp-24-4473-2024, 2024.

Bali, K., Banerji, S., Campbell, J. R., Bhakta, A. V., Chen, L. W. A., Holmes, C. D., and Mao, J.: Measurements of brown carbon and its optical properties from boreal forest fires in Alaska summer, Atmos. Environ., 324, 120436, https://doi.org/10.1016/j.atmosenv.2024.120436, 2024.

Bates, J. T., Fang, T., Verma, V., Zeng, L., Weber, R. J., Tolbert, P. E., Abrams, J. Y., Sarnat, S. E., Klein, M., Mulholland, J. A., and Russell, A. G.: Review of Acellular Assays of Ambient Particulate Matter Oxidative Potential: Methods and Relationships with Composition, Sources, and Health Effects, Environ. Sci. Technol., 53, 4003–4019, https://doi.org/10.1021/acs.est.8b03430, 2019.

Bhattu, D., Tripathi, S. N., Bhowmik, H. S., Moschos, V., Lee, C. P., Rauber, M., Salazar, G., Abbaszade, G., Cui, T., Slowik,

J. G., Vats,, P., Mishra, S., Lalchandani, V., Satish, R., Rai, P., Casotto, R., Tobler, A., Kumar, V., Hao, Y., Qi, L., Khare, P., Manousakas, M., Wang, Q., Han, Y., Tian, J., Darfeuil, S., Minguillon, M., Hueglin, C., Conil, S., Rastogi, N., Srivastava, A., Ganguly, D., Bjelic, S., Canonaco, F., Schnelle-Kreis, J., Dominutti, P. A., Jaffrezo, J., Szidat, S., Chen, Y., Cao, J., Baltensperger, U., Uzu, G., Daellenbach, K. R., Haddad, I., and Prévôt, A. S. H.: Local incomplete combustion emissions define the $PM_{2.5}$ oxidative potential in Northern India, Nat. Commun., 15, 3517, https://doi.org/10.1038/s41467-024-47785-5, 2024.

Bikkina, P., Sarma, V. V. S. S., Kawamura, K., Bikkina, S., Kunwar, B., and Sherin, C. K.: Chemical characterization of wintertime aerosols over the Arabian Sea: Impact of marine sources and long-range transport, Atmos. Environ., 239, 117749, https://doi.org/10.1016/j.atmosenv.2020.117749, 2020.

Cai, J., Zeng, X., Zhi, G., Gligorovski, S., Sheng, G., Yu, Z., Wang, X., and Peng, P.: Molecular composition and photochemical evolution of water-soluble organic carbon (WSOC) extracted from field biomass burning aerosols using high-resolution mass spectrometry, Atmos. Chem. Phys., 20, 6115–6128, https://doi.org/10.5194/acp-20-6115-2020, 2020.

Cao, T., Li, M., Zou, C., Fan, X., Song, J., Jia, W., Yu, C., Yu, Z., and Peng, P.: Chemical composition, optical properties, and oxidative potential of water- and methanol-soluble organic compounds emitted from the combustion of biomass materials and coal, Atmos. Chem. Phys., 21, 13187–13205, https://doi.org/10.5194/acp-21-13187-2021, 2021.

Cao, T., Li, M., Xu, C., Song, J., Fan, X., Li, J., Jia, W., and Peng, P.: Technical note: Chemical composition and source identification of fluorescent components in atmospheric water-soluble brown carbon by excitation–emission matrix spectroscopy with parallel factor analysis – potential limitations and applications, Atmos. Chem. Phys., 23, 2613–2625, https://doi.org/10.5194/acp-23-2613-2023, 2023.

Carena, L., Zoppi, B., Sordello, F., Fabbri, D., Minella, M., and Minero, C.: Phototransformation of Vanillin in Artificial Snow by Direct Photolysis and Mediated by Nitrite, Environ. Sci. Technol., 57, 8785–8795, https://doi.org/10.1021/acs.est.3c01931, 2023.

Casotto, R., Skiba, A., Rauber, M., Strahl, J., Tobler, A., Bhattu, D., Lamkaddam, H., Manousakas, M. I., Salazar, G., Cui, T., Canonaco, F., Samek, L., Ryś, A., Haddad, I. E., Kasper-Giebl, A., Baltensperger, U., Necki, J., Szidat, S., Styszko, K., Slowik, J. G., Prévôt, A. S. H., and Daellenbach, K. R.: Organic aerosol sources in Krakow, Poland, before implementation of a solid fuel residential heating ban, Sci. Total. Environ., 855, 158655, https://doi.org/10.1016/j.scitotenv.2022.158655, 2023.

Ceamanos, X., Coopman, Q., George, M., Riedi, J., Parrington, M., and Clerbaux, C.: Remote sensing and model analysis of biomass burning smoke transported across the Atlantic during the 2020 Western US wildfire season, Sci. Rep., 13, 16014, https://doi.org/10.1038/s41598-023-39312-1, 2023.

Chen, Q., Miyazaki, Y., Kawamura, K., Matsumoto, K., Coburn, S., Volkamer, R., Iwamoto, Y., Kagami, S., Deng, Y., Ogawa, S., Ramasamy, S., Kato, S., Ida, S., Kajii, Y., and Mochida, M.: Characterization of Chromophoric Water-Soluble Organic Matter in Urban, Forest, and Marine Aerosols by HR-ToF-AMS Analysis and Excitation-Emission Matrix Spectroscopy, Environ. Sci. Technol., 50, 10351–10360, https://doi.org/10.1021/acs.est.6b01643, 2016.

Chen, Q., Wang, M., Wang, Y., Zhang, L., Li, Y., and Han, Y.: Oxidative Potential of Water-Soluble Matter Associated with Chromophoric Substances in $PM_{2.5}$ over Xi'an, China, Environ. Sci. Technol., 53, 8574–8584, https://doi.org/10.1021/acs.est.9b01976, 2019.

Choudhary, V., Gupta, T., and Zhao, R.: Evolution of Brown Carbon Aerosols during Atmospheric Long-Range Transport in the South Asian Outflow and Himalayan Cryosphere, ACS Earth. Space. Chem., 6, 2335–2347, https://doi.org/10.1021/acsearthspacechem.2c00047, 2022.

Dasari, S., Andersson, A., Bikkina, S., Holmstrand, H., Budhavant, K., Satheesh, S., Asmi, E., Kesti, J., Backman, J., Salam, A., Bisht, D. S., Tiwari, S., Hameed, Z., and Gustafsson, Ö.: Photochemical degradation affects the light absorption of water-soluble brown carbon in the South Asian outflow, Sci. Adv., 5, eaau8066, https://doi.org/10.1126/sciadv.aau8066, 2019.

Fan, J., Duan, T., Zou, L., and Sun, J.: Characteristics of dissolved organic matter composition in biochar: Effects of feedstocks and pyrolysis temperatures, Environ. Sci. Pollut. Res., 30, 85139–85153, https://doi.org/10.1007/s11356-023-28431-x, 2023.

Fan, X., Cai, F., Xu, C., Yu, X., Wang, Y., Xiao, X., Ji, W., Cao, T., Song, J., and Peng, P.: Molecular weight-dependent abundance, absorption, and fluorescence characteristics of water-soluble organic matter in atmospheric aerosols, Atmos. Environ., 247, 118159, https://doi.org/10.1016/j.atmosenv.2020.118159, 2021.

Fan, X., Xie, S., Yu, X., Cheng, A., Chen, D., Ji, W., Liu, X., Song, J., and Peng, P.: Molecular-level transformations of biomass burning-derived water-soluble organic carbon during dark aqueous OH oxidation: Insights from absorption, fluorescence, high-performance size exclusion chromatography and high-resolution mass spectrometry analysis, Sci. Total. Environ., 912, 169290, https://doi.org/10.1016/j.scitotenv.2023.169290, 2024.

Gallo, F., Uin, J., Sanchez, K. J., Moore, R. H., Wang, J., Wood, R., Mei, F., Flynn, C., Springston, S., Azevedo, E. B., Kuang, C., and Aiken, A. C.: Long-range transported continental aerosol in the eastern North Atlantic: three multiday event regimes influence cloud condensation nuclei, Atmos. Chem. Phys., 23, 4221–4246, https://doi.org/10.5194/acp-23-4221-2023, 2023.

Go, B. R., Li, Y. J., Huang, D. D., and Chan, C. K.: Aqueous-Phase Photoreactions of Mixed Aromatic Carbonyl Photosensitizers Yield More Oxygenated, Oxidized, and less Light-Absorbing Secondary Organic Aerosol (SOA) than Single Systems, Environ. Sci. Technol., 58, 7924–7936, https://doi.org/10.1021/acs.est.3c10199, 2024.

Gu, X., Chen, B., Liu, H., Feng, Y., Wang, B., He, S., Feng, M., Pan, G., and Han, S.: Photochemical behavior of dissolved organic matter derived from Alternanthera philoxeroides hydrochar: Insights from molecular transformation and photochemically reactive intermediates, J. Hazard. Mater., 461, 132591, https://doi.org/10.1016/j.jhazmat.2023.132591, 2024.

He, T., Wu, Y., Wang, D., Cai, J., Song, J., Yu, Z., Zeng, X., and Peng, P.: Molecular compositions and optical properties of water-soluble brown carbon during the autumn and winter in Guangzhou, China, Atmos. Environ., 296, 119573, https://doi.org/10.1016/j.atmosenv.2022.119573, 2023.

He, W. and Hur, J.: Conservative behavior of fluorescence EEM-PARAFAC components in resin fractionation processes and its

applicability for characterizing dissolved organic matter, Water. Res., 83, 217–226, https://doi.org/10.1016/j.watres.2015.06.044, 2015.

Hems, R. F., Schnitzler, E. G., Liu-Kang, C., Cappa, C. D., and Abbatt, J. P. D.: Aging of Atmospheric Brown Carbon Aerosol, ACS Earth. Space. Chem., 5, 722–748, https://doi.org/10.1021/acsearthspacechem.0c00346, 2021.

Hu, T., Luo, M., Qi, Y., He, D., Chen, L., Xu, Y., and Chen, D.: Molecular evidence for the production of labile, sulfur-bearing dissolved organic matter in the seep sediments of the South China Sea, Water. Res., 233, 119732, https://doi.org/10.1016/j.watres.2023.119732, 2023.

Huang, S., Luo, Y., Wang, X., Zhang, T., Lei, Y., Zeng, Y., Sun, J., Che, H., Xu, H., Cao, J., and Shen, Z.: Optical properties, chemical functional group, and oxidative activity of different polarity levels of water-soluble organic matter in $PM_{2.5}$ from biomass and coal combustion in rural areas in Northwest China, Atmos. Environ., 283, 119179, https://doi.org/10.1016/j.atmosenv.2022.119179, 2022.

Jiang, H., Cai, J., Feng, X., Chen, Y., Wang, L., Jiang, B., Liao, Y., Li, J., Zhang, G., Mu, Y., and Chen, J.: Aqueous-Phase Reactions of Anthropogenic Emissions Lead to the High Chemodiversity of Atmospheric Nitrogen-Containing Compounds during the Haze Event, Environ. Sci. Technol., 57, 16500–16511, https://doi.org/10.1021/acs.est.3c06648, 2023.

Laszakovits, J. R., Berg, S. M., Anderson, B. G., O'Brien, J. E., Wammer, K. H., and Sharpless, C. M.: p-Nitroanisole/pyridine and p-nitroacetophenone/pyridine actinometers revisited: quantum yield in comparison to ferrioxalate, Environ. Sci. Technol. Lett., 4, 11–14, https://doi.org/10.1021/acs.estlett.6b00422, 2016.

Lee, H. J., Aiona, P. K., Laskin, A., Laskin, J., and Nizkorodov, S. A.: Effect of solar radiation on the optical properties and molecular composition of laboratory proxies of atmospheric brown carbon, Environ. Sci. Technol., 48, 10217–10226, https://doi.org/10.1021/es502515r, 2014.

Lee, W. C., Deng, Y., Zhou, R., Itoh, M., Mochida, M., and Kuwata, M.: Water Solubility Distribution of Organic Matter Accounts for the Discrepancy in Hygroscopicity among Sub- and Supersaturated Humidity Regimes, Environ. Sci. Technol., 56, 17924–17935, https://doi.org/10.1021/acs.est.2c04647, 2022.

Li, F., Tang, S., Lv, J., He, A., Wang, Y., Liu, S., Cao, H., Zhao, L., Wang, Y., and Jiang, G.: Molecular-Scale Investigation on the Formation of Brown Carbon Aerosol via Iron-Phenolic Compound Reactions in the Dark, Environ. Sci. Technol., 57, 11173–11184, https://doi.org/10.1021/acs.est.3c04263, 2023.

Li, M., Fan, X., Zhu, M., Zou, C., Song, J., Wei, S., Jia, W., and Peng, P.: Abundances and light absorption properties of brown carbon emitted from residential coal combustion in China, Environ. Sci. Technol., 53, 595–603, https://doi.org/10.1021/acs.est.8b05630, 2018.

Liu, C., Chen, D., and Chen, X.: Atmospheric Reactivity of Methoxyphenols: A Review, Environ. Sci. Technol., 56, 2897–2916, https://doi.org/10.1021/acs.est.1c06535, 2022a.

Liu, J., Chang, M., Cheng, Z., Zhu, S., Ding, P., Liu, F., Li, J., and Zhang, G.: High Contribution of South Asian Biomass Burning to Southeastern Tibetan Plateau Air: New Evidence from Radiocarbon Measurement, Environ. Sci. Technol. Lett., 8, 1026–1031, https://doi.org/10.1021/acs.estlett.1c00860, 2021.

Liu, Y., Wang, M., Yin, S., Xie, L., Qu, X., Fu, H., Shi, Q., Zhou, F., Xu, F., Tao, S., and Zhu, D.: Comparing Photoactivities of Dissolved Organic Matter Released from Rice Straw-Pyrolyzed Biochar and Composted Rice Straw, Environ. Sci. Technol., 56, 2803–2815, https://doi.org/10.1021/acs.est.1c08061, 2022b.

Malavelle, F. F., Haywood, J. M., Mercado, L. M., Folberth, G. A., Bellouin, N., Sitch, S., and Artaxo, P.: Studying the impact of biomass burning aerosol radiative and climate effects on the Amazon rainforest productivity with an Earth system model, Atmos. Chem. Phys., 19, 1301–1326, https://doi.org/10.5194/acp-19-1301-2019, 2019.

Manfrin, A., Nizkorodov, S. A., Malecha, K. T., Getzinger, G. J., McNeill, K., and Borduas-Dedekind, N.: Reactive Oxygen Species Production from Secondary Organic Aerosols: The Importance of Singlet Oxygen, Environ. Sci. Technol., 53, 8553–8562, https://doi.org/10.1021/acs.est.9b01609, 2019.

Murphy, K. R., Stedmon, C. A., Graeber, D., and Bro, R.: Fluorescence spectroscopy and multi-way techniques, PARAFAC. Anal. Meth., 5, 6557, https://doi.org/10.1039/c3ay41160e, 2013.

Murphy, K. R., Timko, S. A., Gonsior, M., Powers, L. C., Wunsch, U. J., and Stedmon, C. A.: Photochemistry Illuminates Ubiquitous Organic Matter Fluorescence Spectra, Environ. Sci. Technol., 52, 11243–11250, https://doi.org/10.1021/acs.est.8b02648, 2018.

Podgorski, D. C., Zito, P., McGuire, J. T., Martinovic-Weigelt, D., Cozzarelli, I. M., Bekins, B. A., and Spencer, R. G. M.: Examining Natural Attenuation and Acute Toxicity of Petroleum-Derived Dissolved Organic Matter with Optical Spectroscopy, Environ. Sci. Technol., 52, 6157–6166, https://doi.org/10.1021/acs.est.8b00016, 2018.

Pucher, M., Wünsch, U., Weigelhofer, G., Murphy, K., Hein, T., and Graeber, D.: staRdom: Versatile Software for Analyzing Spectroscopic Data of Dissolved Organic Matter in R, Water, 11, 11, https://doi.org/10.3390/w11112366, 2019.

Schnitzler, E. G., Gerrebos, N. G. A., Carter, T. S., Huang, Y., Heald, C. L., Bertram, A. K., and Abbatt, J. P. D.: Rate of atmospheric brown carbon whitening governed by environmental conditions, P. Natl. Acad. Sci. USA, 119, e2205610119, https://doi.org/10.1073/pnas.2205610119, 2022.

Smith, J. D., Kinney, H., and Anastasio, C.: Phenolic carbonyls undergo rapid aqueous photodegradation to form low-volatility, light-absorbing products, Atmos. Environ., 126, 36–44, https://doi.org/10.1016/j.atmosenv.2015.11.035, 2016.

Song, J., Li, M., Jiang, B., Wei, S., Fan, X., and Peng, P.: Molecular Characterization of Water-Soluble Humic like Substances in Smoke Particles Emitted from Combustion of Biomass Materials and Coal Using Ultrahigh-Resolution Electrospray Ionization Fourier Transform Ion Cyclotron Resonance Mass Spectrometry, Environ. Sci. Technol., 52, 2575–2585, https://doi.org/10.1021/acs.est.7b06126, 2018.

Song, J., Li, M., Fan, X., Zou, C., Zhu, M., Jiang, B., Yu, Z., Jia, W., Liao, Y., and Peng, P.: Molecular Characterization of Water- and Methanol-Soluble Organic Compounds Emitted from Residential Coal Combustion Using Ultrahigh-Resolution Electrospray Ionization Fourier Transform Ion Cyclotron Resonance Mass Spectrometry, Environ. Sci. Technol., 53, 13607–13617, https://doi.org/10.1021/acs.est.9b04331, 2019.

Song, J., Li, M., Zou, C., Cao, T., Fan, X., Jiang, B., Yu, Z., Jia, W., and Peng, P.: Molecular Characterization of Nitrogen-Containing

Compounds in Humic-like Substances Emitted from Biomass Burning and Coal Combustion, Environ. Sci. Technol., 56, 119–130, https://doi.org/10.1021/acs.est.1c04451, 2022.

Sumlin, B. J., Pandey, A., Walker, M. J., Pattison, R. S., Williams, B. J., and Chakrabarty, R. K.: Atmospheric Photooxidation Diminishes Light Absorption by Primary Brown Carbon Aerosol from Biomass Burning, Environ. Sci. Technol. Lett., 4, 540–545, https://doi.org/10.1021/acs.estlett.7b00393, 2017.

Sun, W., Guo, Z., Peng, X., Lin, J., Fu, Y., Yang, Y., Zhang, G., Jiang, B., Liao, Y., Chen, D., Wang, X., and Bi, X.: Molecular characteristics, sources and transformation of water-insoluble organic matter in cloud water, Environ. Pollut., 325, 121430, https://doi.org/10.1016/j.envpol.2023.121430, 2023.

Sun, Y., Zhang, Q., Zheng, M., Ding, X., Edgerton, E. S., and Wang, X.: Characterization and source apportionment of water-soluble organic matter in atmospheric fine particles ($PM_{2.5}$) with high-resolution aerosol mass spectrometry and GC-MS, Environ. Sci. Technol., 45, 4854–4861, https://doi.org/10.1021/es200162h, 2011.

Tang, J., Li, J., Su, T., Han, Y., Mo, Y., Jiang, H., Cui, M., Jiang, B., Chen, Y., Tang, J., Song, J., Peng, P., and Zhang, G.: Molecular compositions and optical properties of dissolved brown carbon in biomass burning, coal combustion, and vehicle emission aerosols illuminated by excitation–emission matrix spectroscopy and Fourier transform ion cyclotron resonance mass spectrometry analysis, Atmos. Chem. Phys., 20, 2513–2532, https://doi.org/10.5194/acp-20-2513-2020, 2020.

Waggoner, D. C., Chen, H. M., Willoughby, A. S., and Hatcher, P. G.: Formation of black carbon-like and alicyclic aliphatic compounds by hydroxyl radical initiated degradation of lignin, Organ. Geochem., 82, 69–76, https://doi.org/10.1016/j.orggeochem.2015.02.007, 2015.

Wang, L., Shen, Z., Lu, D., Zhang, Q., Zhang, T., Lei, Y., and Xu, H.: Water-soluble components in rainwater over Xi'an in northwest China: Source apportionment and pollution controls effectiveness evaluation, Atmos. Pollut. Res., 10, 395–403, https://doi.org/10.1016/j.apr.2018.08.011, 2019.

Wong, J. P. S., Nenes, A., and Weber, R. J.: Changes in Light Absorptivity of Molecular Weight Separated Brown Carbon Due to Photolytic Aging, Environ. Sci. Technol., 51, 8414–8421, https://doi.org/10.1021/acs.est.7b01739, 2017.

Wong, J. P. S., Tsagkaraki, M., Tsiodra, I., Mihalopoulos, N., Violaki, K., Kanakidou, M., Sciare, J., Nenes, A., and Weber, R. J.: Effects of Atmospheric Processing on the Oxidative Potential of Biomass Burning Organic Aerosols, Environ. Sci. Technol., 53, 6747–6756, https://doi.org/10.1021/acs.est.9b01034, 2019.

Yan, W., Chen, Y., Han, L., Sun, K., Song, F., Yang, Y., and Sun, H.: Pyrogenic dissolved organic matter produced at higher temperature is more photoactive: Insight into molecular changes and reactive oxygen species generation, J. Hazard. Mater., 425, https://doi.org/10.1016/j.jhazmat.2021.127817, 2022.

Yang, J., Au, W. C., Law, H., Lam, C. H., and Nah, T.: Formation and evolution of brown carbon during aqueous-phase nitrate-mediated photooxidation of guaiacol and 5-nitroguaiacol, Atmos. Environ., 254, 118401, https://doi.org/10.1016/j.atmosenv.2021.118401, 2021.

Ye, Z., Zhuang, Y., Chen, Y., Zhao, Z., Ma, S., Huang, H., Chen, Y., and Ge, X.: Aqueous-phase oxidation of three phenolic compounds by hydroxyl radical: Insight into secondary organic aerosol formation yields, mechanisms, products and optical properties, Atmos. Environ., 223, 117240, https://doi.org/10.1016/j.atmosenv.2019.117240, 2020.

Ye, Z., Hu, D., Wang, Z., Wang, H., and Ge, X.: Aqueous photochemical aging of water-soluble smoke particles from crop straws burning, Atmos. Environ., 340, 120879, https://doi.org/10.1016/j.atmosenv.2024.120897, 2025.

Zhang, B., Shen, Z., He, K., Sun, J., Huang, S., Xu, H., Li, J., Ho, S. S. H., and Cao, J.: Insight into the Primary and Secondary Particle-Bound Methoxyphenols and Nitroaromatic Compound Emissions from Solid Fuel Combustion and the Updated Source Tracers, Environ. Sci. Technol., 57, 14280–14288, https://doi.org/10.1021/acs.est.3c04370, 2023.

Zhang, R., Gen, M., Liang, Z., Li, Y. J., and Chan, C. K.: Photochemical Reactions of Glyoxal during Particulate Ammonium Nitrate Photolysis: Brown Carbon Formation, Enhanced Glyoxal Decay, and Organic Phase Formation, Environ. Sci. Technol., 56, 1605–1614, https://doi.org/10.1021/acs.est.1c07211, 2022.

Zhao, R., Lee, A. K. Y., Huang, L., Li, X., Yang, F., and Abbatt, J. P. D.: Photochemical processing of aqueous atmospheric brown carbon, Atmos. Chem. Phys., 15, 6087–6100, https://doi.org/10.5194/acp-15-6087-2015, 2015.

Zhao, R., Zhang, Q., Xu, X., Wang, W., Zhao, W., Zhang, W., and Zhang, Y.: Effect of photooxidation on size distribution, light absorption, and molecular compositions of smoke particles from rice straw combustion, Environ. Pollut., 311, 119950, https://doi.org/10.1016/j.envpol.2022.119950, 2022.

Zheng, J., Hu, M., Du, Z., Shang, D., Gong, Z., Qin, Y., Fang, J., Gu, F., Li, M., Peng, J., Li, J., Zhang, Y., Huang, X., He, L., Wu, Y., and Guo, S.: Influence of biomass burning from South Asia at a high-altitude mountain receptor site in China, Atmos. Chem. Phys., 17, 6853–6864, https://doi.org/10.5194/acp-17-6853-2017, 2017.

Zou, C., Cao, T., Li, M., Song, J., Jiang, B., Jia, W., Li, J., Ding, X., Yu, Z., Zhang, G., and Peng, P.: Measurement report: Changes in light absorption and molecular composition of water-soluble humic-like substances during a winter haze bloom-decay process in Guangzhou, China, Atmos. Chem. Phys., 23, 963–979, https://doi.org/10.5194/acp-23-963-2023, 2023.